ChemPubSoc Europe

DOI: 10.1002/cssc.201201001

Catalytic Characteristics of AgCu Bimetallic Nanoparticles in the Oxygen Reduction Reaction

Kihyun Shin,[a] Da Hye Kim,[b] and Hyuck Mo Lee*[a]

Intensive research on oxygen reduction reaction (ORR) catalysts has been undertaken to find a Pt substitute or reduce the amount of Pt. Ag nanoparticles are potential Pt substitutes; however, the weak oxygen adsorption energy of Ag prompted investigation of other catalysts. Herein, we prepared AgCu bimetallic nanoparticle (NP) systems to improve the catalytic performance and compared the catalytic performance of Ag, Cu, AgCu (core–shell), and AgCu (alloy) NP systems as new catalyst by investigating the adsorption energy of oxygen and the activation energy of oxygen dissociation, which is known to be the rate-determining step of ORR. By analyzing HOMO-level isosurfaces of metal NPs and oxygen, we found that the adsorption sites and the oxygen adsorption energies varied with different configurations of NPs. We then plotted the oxygen adsorption energies against the energy barrier of oxygen dissociation to determine the catalytic performance. AgCu (alloy) and Cu NPs exhibited strong adsorption energies and low activation-energy barriers. However, the overly strong oxygen adsorption energy of Cu NPs hindered the ORR.

Introduction

To overcome environmental problems, such as the greenhouse effect,[1] and develop new energy-conversion techniques using renewable sources, many researchers are working on proton-exchange membrane fuel cells (PEMFCs), solar cells, and other technologies. Among the various research topics related to energy-conversion techniques, PEMFCs have attracted the attention of many groups. PEMFCs have a high energy-conversion efficiency (about 50% or higher)[2] and can provide energy for transport vehicles and portable electronic devices.[3] Moreover, hydrogen and oxygen gases are used and water is the only product of the reaction in PEMFCs at low temperatures (<373 K[4]), and they are not harmful to the environment.

The most crucial part of PEMFCs operated at low temperatures is the catalyst that transforms oxygen to water in the cathode; the performance of this catalyst determines the efficiency of the whole PEMFC. Thus, one of the most important issues is the design of a stable and active oxygen reduction reaction (ORR) catalyst to increase the reaction rate in PEMFCs. In practice, noble metals such as Pt are generally used as ORR catalyst;[5–7] however, the amount of Pt in the earth's crust is limited. Thus, Pt scarcity is one of the bottlenecks of PEMFC technology. In addition, typical Pt loadings in the electrode are about 0.4–0.8 mg cm^{-2}.[4] However, the US department of energy (DOE) has set a target of 0.2 mg cm^{-2} to be reached until 2015.[8] To satisfy the DOE target without a significant loss of performance, many research groups have worked to find Pt substitutes or reduce the amount of Pt required by using alloys[9–14] or bimetallic nanoparticles (NPs)[10,15–19] that have a higher activity than bulk materials. The Nørskov group has already investigated the catalytic performance of most transition-metal surfaces and reported that Pt is the best material; thus a new approach is needed to substitute Pt.[20] We chose a bimetallic NP system as a substitute for Pt. Much attention has been focused on Ag, one of the least expensive noble metals;[21–25] however, its weak oxygen adsorption energy[26] led to the investigation of other materials. For this reason, we produced a bimetallic NP from Cu and Ag to strengthen the catalyst's oxygen adsorption energy. Moreover, the cost of Ag and Cu is much lower than that of Pt or Au. In November 2012, the prices of Ag, Cu, Pt, and Au were approximately \$27.0, \$0.3, \$1432.1, and \$1584.8 per troy oz, respectively.[27]

The interest in the use of NPs in various catalyst systems[17,24,28–32] has increased since the pioneering discoveries of the Haruta group, who revealed that Au NPs can catalyze CO oxidation at or below room temperature.[28,33] Before we investigated the catalytic performance of a NP system, we had to confirm its durability[34–38] because durability is an important factor in catalyst design. At this point, we also considered the support, other gases, and acidic conditions involved with the NPs to account for the real conditions in a fuel-cell cathode and confirm its durability and activity; however, it is almost impossible to calculate all of these conditions because of computational limitations. Therefore, we considered the surface tension of the metal element (Ag and Cu) and various isomers consisting of the same number of atoms to determine the energetically most stable structure of the NP system. We initially had to understand the exact reaction mechanism and the

[a] K. Shin, Prof. H. M. Lee
Department of Materials Science & Engineering
Korea Advanced Institute of Science & Technology (KAIST)
373-1 Guseong-dong, Yuseong-gu, Daejeon 305-701 (Korea)
E-mail: hmlee@kaist.ac.kr

[b] Dr. D. H. Kim
Green Transformation Technology Center
Korea Institute of Industrial Technology (KITECH)
711, Hosan-dong, Dalseo-gu, Daegu 704-230 (Korea)

effect of alloying to design noble-metal catalyst systems. Thus, we focused on the effect of structure and alloying.

We used DFT calculations to investigate the ORR using our NP catalyst. Generally, NPs of 2–5 nm in diameter are used in fuel-cell applications.[5,6,39,40] Therefore, it is not easy to control the system, observe the reaction, or identify the reaction mechanism using experimental tools. By applying DFT calculations to nanosized catalysts, we may make observations that are otherwise difficult to do experimentally. In this way, we are going to design a new catalyst.

Results and Discussion

Structural stability of AgCu bimetallic NPs

The truncated octahedron (TOh) structure of NPs (Figure 1) has two layers: a core layer and a shell layer. The core layer consists of six atoms, and the shell layer consists of 32 atoms. Thus, a substitution of the Ag NP core layer by Cu atoms would easily result in the formation of a AgCu (core–shell) NP system. However, the AgCu (alloy) system presented a different challenge. This system has 32 Ag atoms in the shell layer. We performed DFT calculations to find a stable AgCu (alloy) NP system. In the shell layer, there are two types of atomic positions, namely, the center and edge (Figure 1 d). The system with one Cu atom placed at the center of the Ag NP shell layer was more stable (by approximately 0.095 eV) than the system with a Cu atom placed on the edge of it. In all cases, the system with the Cu atoms positioned at the center of the Ag NP shell layer was more stable than other systems with more Cu atoms substituted into the system.

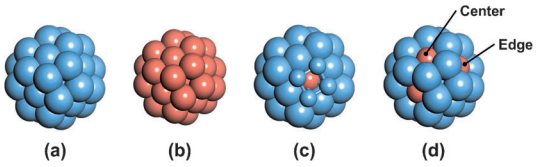

Figure 1. (a) Ag, (b) Cu, (c) AgCu (core–shell), and (d) AgCu (alloy) NPs prepared for calculation; the energy of AgCu (alloy) is higher (1.359 eV) than that of AgCu (core–shell); Ag and Cu NPs are composed of 38 atoms of each element; AgCu (core–shell) and AgCu (alloy) NPs are composed of 32 atoms of Ag and six atoms of Cu.

In these NP systems, the AgCu (core–shell) NP is more stable (by approximately 1.359 eV) than the AgCu (alloy) due to the surface-energy difference between Ag and Cu. In general, an element with a high surface energy is favored to occupy the core layer because it is unstable when that element occupies the shell layer. The surface energy of Cu (1.77 $J m^{-2}$) is higher than that of Ag (1.32 $J m^{-2}$).[41] Thus, the energy of AgCu (core–shell) is lower than that of AgCu (alloy) because Cu atoms are favored to occupy the core layer of the given NP system. Although the AgCu (alloy) NP system is unstable, we evaluated its catalytic performance because it was possible to synthesize this system experimentally.[42] It was important to consider every possible configuration because AgCu (core–shell) and AgCu (alloy) NPs can be synthesized, and the size and shape of the NPs can also be controlled.

Adsorption trends of the oxygen molecule in NP systems

ORR continuously occurs in the cathode of fuel cells; the adsorption energy of the oxygen molecule and the activation-energy barrier of the oxygen dissociation reaction are important aspects of ORR. Oxygen molecule adsorption and dissociation must be considered to determine the performance of a catalyst in ORR. To investigate the oxygen dissociation reaction, we first had to consider oxygen molecule adsorption. There were many different aspects relative to our previous study with thirteen-atom NPs[26] in terms of oxygen molecule adsorption to the NPs. Herein, we considered the stable adsorption site, adsorption energy, and alloying effect on oxygen adsorption.

We considered 8–14 initial adsorption sites to determine stable and strong adsorption sites and obtained reliable calculation results. In Figure 2, the five optimal adsorption sites of the oxygen molecule (R1, R2, R3, R4, and R5) and adsorption sites of the oxygen atom (P1, P2, P3, P4, and P5) are shown. The R1 site represents the square$_{100}$ (s_{100}) site, which shows the oxygen molecule adsorbed symmetrically on the (100) surface. The R4 site represents the bridge (b) site, which shows the oxygen molecule adsorbed on the edge of NPs. The R2, R3, and R5 sites represent the hollow-top (h-t), top-bridge-top (t-b-t), and square$_{111}$ (s_{111}) sites, respectively, which show the molecule adsorbed on the (111) surface. There is a small structural change when the molecule is adsorbed to the R5 (s_{111}) site, which looks like the R1 (s_{100}) site. All the adsorption sites of the oxygen atom are chosen to easily dissociate the oxygen molecule. Each oxygen molecule adsorption site corresponds

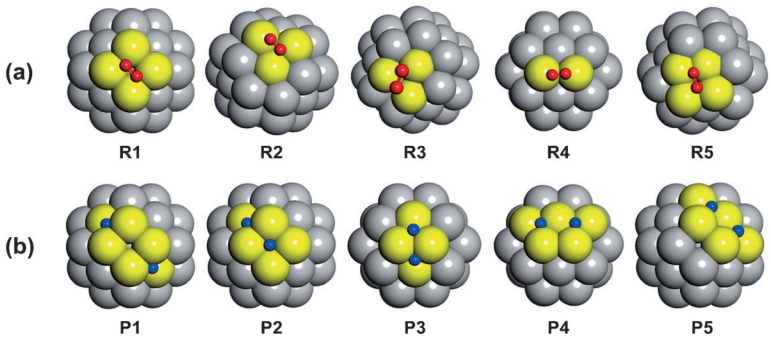

Figure 2. (a) There are five stable adsorption sites (R1, R2, R3, R4, and R5) of an oxygen molecule (red circles) in every NP system: R1 is the square$_{100}$ (s_{100}) site, R2 is the hollow-top (h-t) site, R3 is the top-bridge-top (t-b-t) site, R4 is the bridge (b) site, and R5 is the square$_{111}$ (s_{111}) site. (b) Configurations P1, P2, P3, P4, and P5; oxygen-atom adsorption sites (blue circles) are based on the oxygen molecule adsorption sites.

to two oxygen atom adsorption sites, which is the result of the oxygen dissociation reaction. For instance, R1 is related to P1 and P2, whereas R2 corresponds to P3 and P4.

The three adsorption sites and energies represented for each NP system exhibit notable trends (Table 1). In the four systems, the shell layers of Ag and AgCu (core–shell) are covered exclusively by Ag atoms (Figure 1). The oxygen-molecule adsorption trends show similar tendencies. R1 is the strongest

Table 1. Oxygen molecule adsorption sites and energy values. Each NP system has three optimal adsorption sites. Another system is the $Ag_{29}Cu_9$ (alloy) NP. More Cu atoms were added to the $Ag_{32}Cu_6$ (alloy) to strengthen the effect of the Cu element.

System	Site	E_{ad} [eV]
Ag_{38}	R1 (s_{100})	−0.544
	R4 (b)	−0.322
	R2 (h-t)	−0.288
Cu_{38}	R1 (s_{100})	−1.725
	R2 (h-t)	−1.217
	R3 (t-b-t)	−1.157
$Ag_{32}Cu_6$ (core–shell)	R1 (s_{100})	−0.338
	R2 (h-t)	−0.105
	R5 (s_{111})	−0.093
$Ag_{32}Cu_6$ (alloy)	R5 (s_{111})	−0.623
	R2 (h-t)	−0.574
	R1 (s_{100})	−0.413
$Ag_{29}Cu_9$ (alloy)	R2 (h-t)	−0.902
	R1 (s_{100})	−0.744
	R5 (s_{111})	−0.708

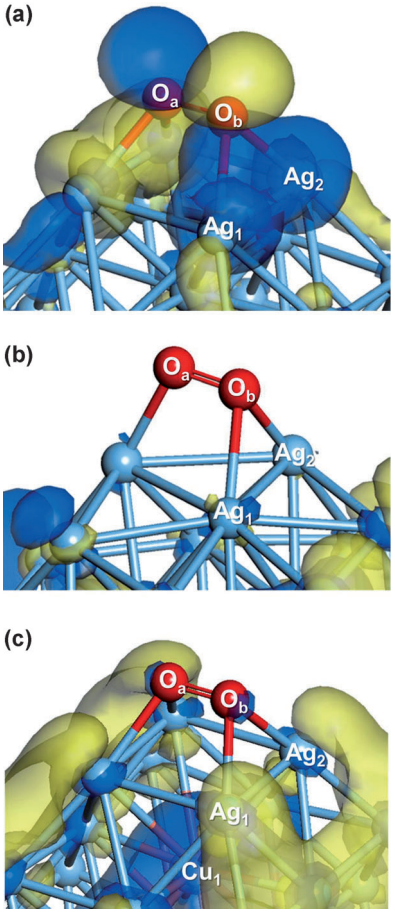

Figure 3. HOMO level isosurface (isovalue = 0.014 e Å) of 38-atom NP systems: (a) R1 site on Ag_{38} NPs; dz^2 orbitals of Ag_1 and Ag_2, which strongly overlap with orbitals of O_a and O_b, are represented. (b) R2 adsorption site on Ag_{38} NPs; it is difficult to find the orbital isosurface between O_b and Ag_1–Ag_2. (c) Oxygen molecule adsorption to $Ag_{32}Cu_6$ (core–shell) NPs.

adsorption site because it has the same shell-layer conditions. However, a previous study on the cuboctahedron (COh) structure of the thirteen-atom NP system showed that the R2 site is the most stable adsorption site among all systems.[21,24] COh and TOh are almost identical structures and have the same face-centered cubic (fcc) symmetry. We drew the HOMO-level isosurface for each system (thirteen and 38 atoms) to analyze the electronic distribution difference between COh and TOh.

The isosurface of the HOMO to the R1 adsorption sites (Figure 3) shows that there is a significant difference between the adsorption to (a) R1 and (b) R2. In the case of the R1 adsorption site, the Ag_1 and Ag_2 atoms directly adsorb to the oxygen molecule to form dz^2-like orbitals in the radial direction from the center of the NP; these dz^2-like orbitals strongly overlap with the orbital of O_b. This result means that the oxygen molecules are strongly bonded to NPs. In contrast with the result of R_1, it is difficult to find the isosurface of the HOMO orbital level in R_2, which means that the oxygen molecules are not strongly adsorbed to the R2 site. In the case of the thirteen-atom NP system, the trends are different. The orbital overlap of R2 is larger than that of R1. Thus, the adsorption-site preference can be altered by adjusting the diameter of the NPs.

Despite the fact that the AgCu (core–shell) NP system is covered only by Ag atoms (similarly to Ag NP systems) the adsorption energy of the oxygen molecule is low. To verify the reason for the weak oxygen molecule adsorption in AgCu (core–shell) NPs, we drew the HOMO orbital level and compared the result to another system. In Figure 3c, the number of electrons is insufficient in Ag_1 and Ag_2 to bond with the oxygen molecule due to the presence of the Cu core. The electrons are highly localized in the Cu core, which causes the oxygen binding energy of AgCu (core–shell) NPs to weaken.

Previously, we reported that the thirteen-atom AgCu (alloy) NP system had a higher adsorption energy than the Ag NP system.[26] In this calculation, however, the adsorption energy of the AgCu (alloy) NP is not improved. The Cu atom positioned at the center of the (111) surface does not participate to a large extent because the charge of this Cu atom is positive (+0.016). In contrast, the charge of the Cu atom occupying the edge of the (111) surface is negative (−0.024); therefore, the Cu atom can donate electrons to the oxygen molecule to help adsorption. Thus, we increased Cu atoms to the $Ag_{32}Cu_6$ (alloy) NP system to verify the effect of positioning on the edge. In Table 1, the oxygen adsorption energy to the $Ag_{29}Cu_9$

(alloy) NP system is represented; the adsorption energy is dramatically increased relative to $Ag_{32}Cu_6$ (alloy) NPs.

Activation energy of oxygen dissociation

Using the calculation results above for oxygen molecule (and atom) adsorption, we investigated the oxygen dissociation reaction with a focus on two aspects of ORR. The first was to achieve a low activation-energy value for oxygen dissociation (to boost ORR), and the second was to achieve a strong adsorption-energy value for oxygen because the ORR occurs after an oxygen molecule is adsorbed to NPs. We considered six reaction pathways based on our calculation results for each NP system and then chose four datasets with low activation energies and strong adsorption energies (Figure 4).

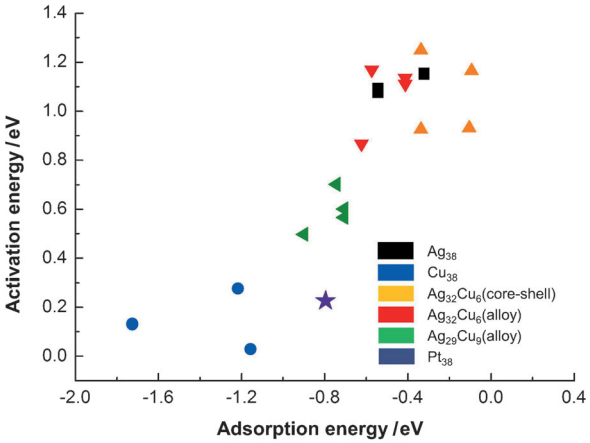

Figure 4. Relationship between the activation energy of oxygen dissociation and the adsorption energy of an oxygen molecule. The *x* axis represents the adsorption energy of an oxygen molecule, whereas the *y* axis represents the activation energy of oxygen dissociation. Black is Ag_{38}, blue is Cu_{38}, orange is $Ag_{32}Cu_6$ (core–shell), red is $Ag_{32}Cu_6$ (alloy), green is $Ag_{29}Cu_9$ (alloy), and purple is Pt_{38} for benchmark.

The lowest activation energies of Ag_{38}, Cu_{38}, $Ag_{32}Cu_6$ (core–shell), $Ag_{32}Cu_6$ (alloy), and $Ag_{29}Cu_9$ (alloy) were 0.905, 0.029, 0.926, 0.702, and 0.497 eV, respectively. From these results, we could control the adsorption energy of the oxygen molecule and activation energy of the oxygen dissociation by varying the composition of Cu. However, to improve this property, we had to add more than eight Cu atoms because the effect of Cu comes from substitution of the edge-position atoms in the TOh structure of the 38-atom NP system.

Cu_{38} and $Ag_{29}Cu_9$ (alloy) NP systems may be good candidates for ORR catalysts based on the results described above because they have strong adsorption energies and low activation energies. However, adsorption of oxygen molecules that is too strong or too weak can reduce the ORR rate.[20] Adsorption of oxygen that is too strong can be an obstacle to the progress of the reaction because strong adsorption implies that it is difficult to desorb. Adsorption that is too weak induces a high activation energy of oxygen dissociation. The adsorption energy of Ag_{38} and the $Ag_{32}Cu_6$ (core–shell) NP system is approximately −0.3 to −0.5 eV, and these weak adsorption energies induce high activation energies (approximately 0.9–1.2 eV). Therefore, Ag_{38} and $Ag_{32}Cu_6$ (core–shell) NP systems are not suitable as ORR catalysts. The Cu_{38} NP system has an adsorption energy (approximately −1.7 eV) that is about three to six times higher than the adsorption energy of Ag_{38} and $Ag_{32}Cu_6$ (core–shell) NP systems. In fact, the Cu NP system has a strong tendency to be oxidized due to overly strong adsorption.[43,44] Although the Cu_{38} NP system has a low activation energy of oxygen dissociation, this system is not appropriate as an ORR catalyst. In contrast to the Cu_{38} NP system, $Ag_{29}Cu_9$ (alloy) has an optimal adsorption-energy and activation-energy barrier. Due to the optimal level of adsorption energy, the $Ag_{29}Cu_9$ (alloy) system can overcome the oxide problem and prevent oxygen atom poisoning. In other experiments, AgCu (alloy) NPs had no oxide layer, although the NP average size was slightly larger.[45]

Comparing the oxygen adsorption energy and activation energy of oxygen dissociation of the $Ag_{29}Cu_9$ (alloy) NP system with those of Pt_{38} NPs, $Ag_{29}Cu_9$ (alloy) and Pt_{38} NPs have similar oxygen adsorption energies (−0.902 and −0.796 eV, respectively). In the case of activation energy, $Ag_{29}Cu_9$ (alloy) has a slightly higher activation energy (0.497 eV) than that of Pt_{38} (0.227 eV). $Ag_{29}Cu_9$ (alloy) may be a good ORR catalyst because $Ag_{29}Cu_9$ (alloy) has an advantage in terms of cost, despite the fact that it has a slightly poorer activity relative to Pt_{38}.

Conclusions

We investigated four systems, including pure Ag_{38} and Cu_{38} NP systems and bimetallic $Ag_{(38-x)}Cu_x$ ($x = 6$, 9) NP systems. $Ag_{32}Cu_6$ (core–shell) is more stable than $Ag_{32}Cu_6$ (alloy) because Cu has a relatively high surface energy relative to Ag.

Oxygen molecules are favored to adsorb to the R1 site in our system, and we found that the highly overlapped orbital makes oxygen bind strongly near the R1 site. $Ag_{32}Cu_6$ (core–shell) has a lower adsorption energy because Cu atoms have highly localized orbitals in the core layer. Highly localized orbitals hinder the donation of an electron to oxygen, causing oxygen binding to be weakened. The position of Cu atoms in the Ag-based NPs affects the strength of oxygen molecule adsorption.

Among the four systems, Cu_{38} and $Ag_{29}Cu_9$ (alloy) NP systems are potential ORR catalysts. However, Cu is easily oxidized because of the high adsorption energy of the oxygen molecule. Thus, the $Ag_{29}Cu_9$ (alloy) NP system seems to be the most suitable ORR catalyst.

Experimental Section

We performed GGA-level spin-polarized Kohn–Sham DFT calculations using the atomic orbital-based DMol^3 package.[46,47] The Kohn–Sham equation was expanded in a double-numerical quality basis set with polarization functions (DNP). The exchange correlation energy was functionalized with the revised PBE (RBPE) functional.[48–51] In general, the RPBE functional was found to be superior in the description of energetics of atomic and molecular bond-

ing to transition metals according to many researchers.[52–54] The orbital cutoff range was set to 5.0 Å. To treat the core electrons of heavy Ag and Cu atoms, we used the DFT semicore pseudopotential.[55] Fermi smearing was set to 0.003 Ha (1 Ha = 27.2114 eV) in all calculations. The convergence tolerances of energy, force, and displacement were 2×10^{-5} Ha, 0.004 Ha Å^{-1}, and 0.005 Å, respectively.

Herein, Ag, Cu, AgCu (core–shell), and AgCu (alloy) NP systems composed of 38 atoms (approximately 1 nm in diameter) were prepared; the structure of the NP systems was TOh, which was one of the stable structures. Generally, NPs of 2–5 nm in diameter were chosen to investigate catalytic activity because of their high activity.[56–58] However, Qiao et al. reported that even NPs of <1 nm in diameter exhibit an extremely high activity.[59] Therefore, we chose a NP system composed of 38 atoms to investigate the catalytic reaction; Pt_{38} NPs of similar diameter were used as a benchmark. Generally, metal NPs were not used as an isolated entity, but were supported by a support material (e.g., metal oxide).[56,60–64] The structure of a supported NP system was commonly a pyramidal one with a fcc symmetry;[56,61–64] the structure of NPs (TOh) herein was similar to that pyramidal one because it also had a fcc symmetry. Thus, we used TOh as the initial structure in the four catalyst systems and performed geometry optimization to find the most stable structure.[23] TOh had six (100) surfaces and eight (111) surfaces and consisted of six atoms in the core and 32 atoms in the shell. In Figure 1, six atoms of Cu occupied the core and 32 atoms of Ag occupied the shell in the AgCu (core–shell) NP system. In the case of AgCu (alloy), six atoms of Cu were located in the center of the (111) surface because location of the Cu atoms in the center of (111) provided the greatest stability in this calculation.

The ORR occurred and generated energy in the PEMFC cathode. Herein, we focused on two aspects of this system, including the activation energy of oxygen dissociation, well-known to be the rate-determining step of the ORR, and the oxygen adsorption energy starting point of the ORR. A good ORR catalyst must lower the activation-energy barrier of oxygen dissociation to boost ORR and has a strong adsorption energy to initiate ORR. Therefore, we performed DFT calculations to investigate the adsorption energy of the oxygen molecule and the activation energy of the oxygen dissociation reaction. To calculate the activation energy of the oxygen dissociation reaction, we needed to know the oxygen molecule adsorption to the reactant and the oxygen atom adsorption to the product. We considered approximately ten adsorption sites for each adsorption calculation to increase the reliability of the calculation results. The adsorption energies (E_{ad}) were calculated using Equation (1):

$$E_{ad} = E_{mol+NP} - E_{NP} - E_{mol} \quad (1)$$

where E_{mol+NP} is the total energy of oxygen-adsorbed NPs, E_{NP} is the total energy of NPs, and E_{mol} is the chemical potential of oxygen.

Using the calculated results of the oxygen molecule (atom) adsorption, we calculated the activation energy of the oxygen dissociation reaction and compared the activation energy and adsorption energy to find the relationship between them.[24,26]

Acknowledgements

This work was supported by the National Research Foundation of Korea (NRF) grant funded by the Korean Government (MEST) (2011-0028612), as well as by the Future-Based Technology Development Program (Nano Fields) through NRF funding by the Ministry of Education, Science, and Technology (2009-0082472)

Keywords: density functional theory · fuel cells · heterogeneous catalysis · nanoparticles · oxygen

[1] T. A. Boden, G. Marland, R. J. Andres, Carbon Dioxide Information Analysis Center, Oak Ridge National Laboratory, US Department of Energy, Oak Ridge, Tenn., USA, **2012**.
[2] A. Hamnett in *Handbook of Fuel Cells—Fundamentals, Technology and Application, Vol. 1*, Wiley, New York, **2003**, p. 34.
[3] R. O'Hayre, S.-W. Cha, W. Colella, F. B. Prinz in *Fuel Cell Fundamentals*, Wiley, Hoboken, NJ, **2006**, p. 8.
[4] H. A. Gasteiger, S. S. Kocha, B. Sompalli, F. T. Wagner, *Appl. Catal. B* **2005**, *56*, 9–35.
[5] J. Zhang, K. Sasaki, E. Sutter, R. R. Adzic, *Science* **2007**, *315*, 220–222.
[6] J. K. Nørskov, T. Bligaard, J. Rossmeisl, C. H. Christensen, *Nat. Chem.* **2009**, *1*, 37–46.
[7] Y. Shao-Horn, W. C. Sheng, S. Chen, P. J. Ferreira, E. F. Holby, D. Morgan, *Top. Catal.* **2007**, *46*, 285–305.
[8] Hydrogen and Fuel Cells Program Records, US Department of Energy http://www.hydrogen.energy.gov/pdfs/9018_platinum_group.pdf.
[9] X. Chen, S. Sun, X. Wang, F. Li, D. Xia, *J. Phys. Chem. C* **2012**, *116*, 22737–22742.
[10] M. H. Seo, S. M. Choi, J. K. Seo, S. H. Noh, W. B. Kim, B. Han, *Appl. Catal. B* **2013**, *129*, 163–171.
[11] A. S. Bondarenko, I. E. L. Stephens, L. Bech, I. Chorkendorff, *Electrochim. Acta* **2012**, *82*, 517–523.
[12] M. Escudero-Escribano, A. Verdaguer-Casadevall, P. Malacrida, U. Grønbjerg, B. P. Knudsen, A. K. Jepsen, J. Rossmeisl, I. E. L. Stephens, I. Chorkendorff, *J. Am. Chem. Soc.* **2012**, *134*, 16476–16479.
[13] V. Di Noto, E. Negro, *Fuel Cells* **2010**, *10*, 234–244.
[14] V. Di Noto, E. Negro, S. Polizzi, F. Agresti, G. A. Giffin, *ChemSusChem* **2012**, *5*, 2451–2459.
[15] L. Zhang, G. Henkelman, *J. Phys. Chem. C* **2012**, *116*, 20860–20865.
[16] F. Godínez-Salomón, M. Hallen-López, O. Solorza-Feria, *Int. J. Hydrogen Energy* **2012**, *37*, 14902–14910.
[17] S. Alayoglu, A. U. Nilekar, M. Mavrikakis, B. Eichhorn, *Nat. Mater.* **2008**, *7*, 333–338.
[18] V. Di Noto, E. Negro, *Electrochim. Acta* **2010**, *55*, 7564–7574.
[19] V. Di Noto, E. Negro, S. Polizzi, P. Riello, P. Atanassov, *Appl. Catal. B* **2012**, *111–112*, 185–199.
[20] J. K. Nørskov, J. Rossmeisl, A. Logadottir, L. Lindqvist, J. R. Kitchin, T. Bligaard, H. Jónsson, *J. Phys. Chem. B* **2004**, *108*, 17886–17892.
[21] H. Y. Kim, S. S. Han, J. H. Ryu, H. M. Lee, *J. Phys. Chem. C* **2010**, *114*, 3156–3160.
[22] D. H. Kim, H. Y. Kim, H. G. Kim, J. H. Ryu, H. M. Lee, *J. Phys. Condens. Matter* **2008**, *20*, 035208.
[23] K. Michaelian, N. Rendón, I. L. Garzón, *Phys. Rev. B* **1999**, *60*, 2000–2010.
[24] D. H. Kim, K. Shin, H. M. Lee, *J. Phys. Chem. C* **2011**, *115*, 24771–24777.
[25] H. Y. Kim, H. M. Lee, G. Henkelman, *J. Am. Chem. Soc.* **2012**, *134*, 1560–1570.
[26] K. Shin, D. H. Kim, S. C. Yeo, H. M. Lee, *Catal. Today* **2012**, *185*, 94–98.
[27] Current Primary and Scrap Metal Price, http://www.metalprices.com.
[28] M. Haruta, T. Kobayashi, H. Sano, N. Yamada, *Chem. Lett.* **1987**, *16*, 405–408.
[29] B. K. Min, C. M. Friend, *Chem. Rev.* **2007**, *107*, 2709–2724.
[30] J. H. Ryu, S. S. Han, D. H. Kim, G. Henkelman, H. M. Lee, *ACS Nano* **2011**, *5*, 8515–8522.
[31] J. H. Ryu, H. Y. Kim, D. H. Kim, D. H. Seo, H. M. Lee, *J. Phys. Chem. C* **2010**, *114*, 2022–2026.
[32] D. H. Seo, H. Y. Kim, J. H. Ryu, H. M. Lee, *J. Phys. Chem. C* **2009**, *113*, 10416–10421.
[33] M. Haruta, *Gold Bull.* **2004**, *37*, 27–36.
[34] H. Y. Kim, H. G. Kim, D. H. Kim, H. M. Lee, *J. Phys. Chem. C* **2008**, *112*, 17138–17142.
[35] D. H. Kim, H. Y. Kim, J. H. Ryu, H. M. Lee, *Phys. Chem. Chem. Phys.* **2009**, *11*, 5079–5085.
[36] H. Y. Kim, H. G. Kim, J. H. Ryu, H. M. Lee, *Phys. Rev. B* **2007**, *75*, 212105.

[37] J. H. Ryu, H. Y. Kim, D. H. Kim, S. K. Choi, H. M. Lee, *J. Nanosci. Nanotechnol.* **2009**, *9*, 2553 – 2557.
[38] S. C. Yeo, D. H. Kim, K. Shin, H. M. Lee, *Phys. Chem. Chem. Phys.* **2012**, *14*, 2791 – 2796.
[39] R. R. Adzic, J. Zhang, K. Sasaki, M. B. Vukmirovic, M. Shao, J. X. Wang, A. U. Nilekar, M. Mavrikakis, J. A. Valerio, F. Uribe, *Top. Catal.* **2007**, *46*, 249 – 262.
[40] M. Turner, V. B. Golovko, O. P. H. Vaughan, P. Abdulkin, A. Berenguer-Murcia, M. S. Tikhov, B. F. G. Johnson, R. M. Lambert, *Nature* **2008**, *454*, 981 – 983.
[41] W. R. Tyson, W. A. Miller, *Surf. Sci.* **1977**, *62*, 267 – 276.
[42] M. Tsuji, S. Hikino, R. Tanabe, D. Yamaguchi, *Chem. Lett.* **2010**, *39*, 334 – 336.
[43] C. S. Choi, Y.-U. Park, H. Kim, N. R. Kim, K. Kang, H. M. Lee, *Electrochim. Acta* **2012**, *70*, 98 – 104.
[44] C. S. Choi, Y. H. Jo, M. G. Kim, H. M. Lee, *Nanotechnology* **2012**, *23*, 065601.
[45] N. S. Tabrizi, Q. Xu, N. M. Pers, A. Schmidt-Ott, *J. Nanopart. Res.* **2010**, *12*, 247 – 259.
[46] B. Delley, *J. Chem. Phys.* **2000**, *113*, 7756 – 7764.
[47] B. Delley, *Comput. Mater. Sci.* **2000**, *17*, 122 – 126.
[48] J. P. Perdew, K. Burke, M. Ernzerhof, *Phys. Rev. Lett.* **1996**, *77*, 3865 – 3868.
[49] J. P. Perdew, K. Burke, M. Ernzerhof, *Phys. Rev. Lett.* **1997**, *78*, 1396 – 1396.
[50] Y. Zhang, W. Yang, *Phys. Rev. Lett.* **1998**, *80*, 890 – 890.
[51] J. P. Perdew, Y. Wang, *Phys. Rev. B* **1992**, *45*, 13244 – 13249.
[52] C. J. Cramer, D. G. Truhlar, *Phys. Chem. Chem. Phys.* **2009**, *11*, 10757 – 10816.
[53] A. Matveev, M. Staufer, M. Mayer, N. Rösch, *Int. J. Quantum Chem.* **1999**, *75*, 863 – 873.
[54] B. Hammer, L. B. Hansen, J. K. Nørskov, *Phys. Rev. B* **1999**, *59*, 7413 – 7421.
[55] B. Delley, *Phys. Rev. B* **2002**, *66*, 155125.
[56] T. Kiyonaga, Q. Jin, H. Kobayashi, H. Tada, *ChemPhysChem* **2009**, *10*, 2935 – 2938.
[57] I. Laoufi, M. C. Saint-Lager, R. Lazzari, J. Jupille, O. Robach, S. Garaudée, G. Cabailh, P. Dolle, H. Cruguel, A. Bailly, *J. Phys. Chem. C* **2011**, *115*, 4673 – 4679.
[58] M. Valden, X. Lai, D. W. Goodman, *Science* **1998**, *281*, 1647 – 1650.
[59] B. Qiao, A. Wang, X. Yang, L. F. Allard, Z. Jiang, Y. Cui, J. Liu, J. Li, T. Zhang, *Nat. Chem.* **2011**, *3*, 634 – 641.
[60] L. Fu, N. Q. Wu, J. H. Yang, F. Qu, D. L. Johnson, M. C. Kung, H. H. Kung, V. P. Dravid, *J. Phys. Chem. B* **2005**, *109*, 3704 – 3706.
[61] Y. Yang, J. Evans, J. A. Rodriguez, M. G. White, P. Liu, *Phys. Chem. Chem. Phys.* **2010**, *12*, 9909 – 9917.
[62] L. Barrio, P. Liu, J. A. Rodriguez, J. M. Campos-Martin, J. L. G. Fierro, *J. Chem. Phys.* **2006**, *125*, 164715 – 164715.
[63] L. Barrio, P. Liu, J. A. Rodriguez, J. M. Campos-Martin, J. L. G. Fierro, *J. Phys. Chem. C* **2007**, *111*, 19001 – 19008.
[64] P. Liu, J. A. Rodriguez, *J. Chem. Phys.* **2007**, *126*, 164705 – 164708.

Received: December 27, 2012
Revised: February 28, 2013
Published online on May 3, 2013